IEEE Access
Multidisciplinary | Rapid Review | Open Access Journal

Received February 5, 2021, accepted March 12, 2021, date of publication March 24, 2021, date of current version June 24, 2021.

Digital Object Identifier 10.1109/ACCESS.2021.3068417

An Intelligent Optimization-Based Particle Filter for Fault Diagnosis

ZHENG CAO[1,2,3] AND XIANJUN DU[1]

[1]College of Electrical and Information Engineering, Lanzhou University of Technology, Lanzhou 730050, China
[2]Key Laboratory of Gansu Advanced Control for Industrial Processes, Lanzhou University of Technology, Lanzhou 730050, China
[3]National Demonstration Center for Experimental Electrical and Control Engineering Education, Lanzhou University of Technology, Lanzhou 730050, China

Corresponding author: Xianjun Du (xdu@lut.edu.cn)

This work was supported in part by the National Natural Science Foundation of China under Grant 61563032, Grant 61763028, and Grant 61963025; in part by the Natural Science Foundation of Gansu Province under Grant 1506RJZA104; and in part by the University Scientific Research Project of Gansu Province under Grant 2015B-030.

ABSTRACT It is very important to implement the fault diagnosis technology in industrial processes to make the process more reliable. In this paper, an improved particle filter (PF) method based on a modified beetle swarm antennae search (BSAS) algorithm is proposed and verified in a doubly fed induction generator (DFIG) fault diagnosis application. Firstly, the search strategy of BSAS is improved to ensure its global search ability. Secondly, it is introduced to the traditional PF algorithm to improve the particle diversity and impoverishment drawbacks. Finally, the fault diagnosis algorithm is verified by combining the DFIG state space model. The simulation experimental of fault detection and isolation results show that the proposed method is simple and effective, and it can effectively monitor the occurrence of faults. For the fault diagnostic application, the method proposed in this paper could be implemented in other model based processes, including chemical process, biochemical wastewater treatment process, etc.

INDEX TERMS Fault diagnosis, detection and isolation, particle filter (PF), beetle swarm antennae search (BSAS) algorithm, doubly fed induction generator (DFIG).

I. INTRODUCTION

Wind energy, a clean and renewable energy, is the fastest-growing energy source in the world in the last decades, which is considered as an effective way to face and solve the world energy problem [1]. 2018 is a good year for wind energy with 51.3 GW newly added capacity worldwide, including 46.8 GW of onshore wind power and 4.5 GW of offshore wind power. Up to 2018, 591.1 GW of wind power has been installed globally, including 23.1 GW offshore installation, which is accounting for 4% of the total installation.

Global wind report 2018 published by Global Wind Energy Council (GWEC), indicates that there would be more than 360 GW new installations and nearly 1000 GW of total installations worldwide by 2023 [2] shown in Figure 1. A report from the International Renewable Energy Agency (IRENA) shows that wind power could cover more than one-third of global power needs (35%) by 2050, becoming the world's foremost generation source [3].

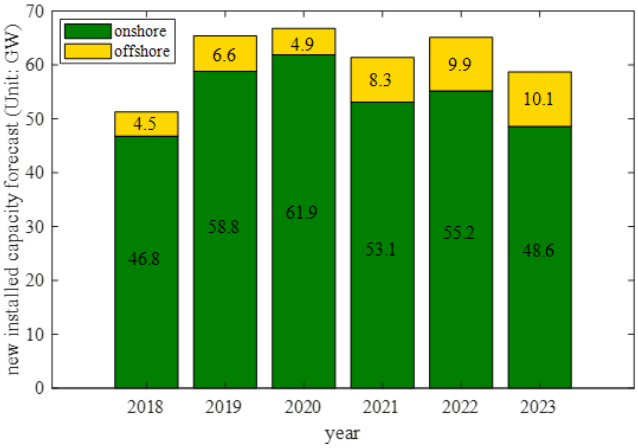

FIGURE 1. 2019-2023 annual forecast of new installed capacity globally. (All the data are collected from Global Wind Report 2018, published by GWEC in April 2019.)

Most wind turbines (WTs) are usually installed in remote areas, e.g. mountainous, countryside, and offshore regions, where the working environment is very harsh. The doubly

The associate editor coordinating the review of this manuscript and approving it for publication was Mark Kok Yew Ng.

fed induction generator (DFIG)-based wind turbine is the key device in wind power generation systems, whose basic functionality is to transfer the wind power into the mechanical power on the rotor shaft. However, with the continuous growth of wind turbine capacity, WT system structure is becoming increasingly complex, and the coupling between different components is more closely. Because of the temperature variation, material corrosion, mechanical stress, and voltage stress, etc., faults could occur unexpectedly at any components of wind turbine systems. It's needless to say that even a small fault may cause a big fault, because all the mechanisms in the system are reacted in chain. That is, a small fault may spread into a catastrophic big fault, causing wind turbine outage, or even directly leading to wind turbine damage, resulting in huge economic losses. Faults in the generator and drive train (includes gear box, main shafts, and bearings) are the most crucial and widely observed failures, which dominate over 60% of the downtime in wind turbine systems [4] in some power plants located in Sweden, Finland, and Germany during 1997-2005, and it is similar to the other countries in the world. Therefore, having a reliable fault diagnosis and fault tolerant control (FTC) scheme is crucial to improve the reliability of wind turbines and reduce expensive repair costs, especially for the offshore wind generators because they are not easily accessible.

Scholars and researchers worldwide have done many researches and applications of the fault diagnostic methods for key parts of wind power generation system, such as gearbox, generator, and other components [5]–[9], based on the three main categories of fault diagnosis: i) signal-based approach, ii) knowledge-based approach and iii) model-based approach. The first two approaches are still commonly used techniques in practice, and the last one has its advantages and should definitely be implemented for practice using in the future.

In model-based approaches, an accurate mathematical model is required to represent the system. Such a model runs in parallel to the system and is supplied with the same input signals. In an ideal situation, the model variables can well track the real system variables in the absence of fault and present an obvious derivation when a fault occurs.

This derivation is measured in terms of a residual, which is obtained by subtracting the measured system variables with their estimates provided by the model. The residual contains important information with respect to the fault. The fault detection and diagnosis can be then achieved by observing and analyzing this residual. A schematic description of the model-based fault detection and diagnosis (FDD) scheme is given in Figure 2, which is accomplished by two steps: the residual generation and residual evaluation [10], [11].

In this paper, an improved particle filter algorithm is proposed for the DFIG fault diagnosis based on the state space DFIG system model. Dynamic adaptive inertia weight is employed to improve the global search capability of the beetle swarm antennae search (BSAS) algorithm, which is used to optimize the resampling process of the typical particle filter algorithm in avoiding the particle degeneracy with the iterations going on.

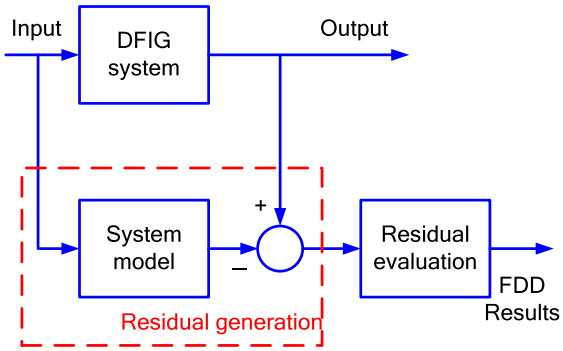

FIGURE 2. Schematic description of the model-based FDD.

II. MATERIALS AND METHODS

A. BASIC THEORY OF PARTICLE FILTER

Particle filter (PF) has been proved that it is an effective method to do the state estimation works based on the state space system model [12]–[15], which uses a set of weighted particles (as well as statistical samples) to approximate the posterior probability density function, and implements recursive Bayesian estimation to estimate the system state by nonparametric Monte Carlo method [16].

According to the sequential importance resampling (SIR) algorithm [14], [17], [18], which is commonly believed as the original PF algorithm, the classical process of state estimation can be summarized as follows:

Assume that the state space model of a nonlinear system is represented as Equations (1) and (2):

$$x_k = f(x_{k-1}, u_k) \tag{1}$$

$$y_k = g(x_k, v_k) \tag{2}$$

where in state Equation (1) and observation Equation (2), f and g represent two nonlinear functions; x_k and y_k are the state and observation vector of the system at time k (assuming x_k obeys the first-order Markov process with the prior initial probability density $p(x_0)$); u_k and v_k are the system state noise and observation noise respectively, which are random variables independent from the system state, and independent of each other as well.

Step 1. Prediction: N particles are extracted from the transition probability density of the system states ($p(x_k|x_{k-1})$).

$$x_k(i) \sim p(x_k|x_{k-1}(i)), \quad i = 1, 2, \cdots, N \tag{3}$$

Step 2. Update: use Equation (4) to update the sample weights and use Equation (5) to normalize them.

$$w_k^*(i) = w_{k-1}^*(i) p(y_k|x_k(i)) \tag{4}$$

$$w_k(i) = \frac{w_k^*(i)}{\sum_{i=1}^{N} w_k^*(i)} \tag{5}$$

where, $p(y_k|x_k)$ is the observed likelihood probability density of the system states.

Step 3. Estimation: use Equation (6) to estimate the value $\hat{x}_k$ of x_k. The least mean square error estimation is performed here.

$$\hat{x}_k = \sum_{i=1}^{N} w_k(i) x_k(i) \tag{6}$$

Step 4. Resampling: perform a multinomial resampling to get a number of N new particles with equal weights. After the resampling process, the particles with small weights are knocked out, and many new particles (which can be considered as offspring) will be obtained from the particles (which can be considered as parents) with big weights.

Compared with the traditional filtering methods, particle filter (PF) has the advantages of simple principle and applicable to a wide environment [19]. It has become an effective method to study optimal estimation problems of non-linear and non-Gaussian dynamic systems, and has been widely used in the fields of machine vision, navigation, parameter estimation, target tracking, state monitoring, and fault diagnosis, etc. [20]–[23].

Everything has two sides, on the one hand, the resampling process can solve the problem of particle degeneracy with new particles produced. However, on the other hand, resampling brings a new problem caused by the mechanism of the resampling procedure, in which only the particles with big weights will be selected as copy samples and the particles with small weights are going to be eliminated [24]. This is called particle impoverishment. To deal with this issue, many improvements have been applied to perfect the PF algorithm [25]–[27].

B. IMPROVED BEETLE SWARM ANTENNAE SEARCH (BSAS) ALGORITHM

1) BSAS ALGORITHM

The beetle swarm antennae search (BSAS) [28] algorithm, an improved version of the beetle antennae search (BAS) algorithm [29], is one of the meta-heuristic algorithms for optimization problems, which is inspired by the searching behavior of long-horn beetles. The BAS algorithm imitates the function of antennae and the random walking mechanism of beetles in nature. The beetle explores the nearby area randomly using both antennae. Each antenna can receive the odor when it is preying or finding mates. The beetle determines the walking direction by judging the concentration of odor received and turns to the higher concentration side for target searching probability.

However, one beetle walks in one random direction each step cannot guarantee the search process is orienting the better value of the objective function. Correspondingly, if we could employ n beetles to move in n directions, the swarm beetles would find a better position more possibly. Another point is we can let the beetle stay at the best position while if there is no better position found after searching move. That is to say, there is a small probability that all the beetles will miss the better position at the current step. Therefore, a probability constant, belongs to [0, 1], is introduced to measure the impact of random directions of the swarm beetles. Based on the above aspects, the basic steps of the BSAS algorithm can be summarized as follows.

Step 1. Initialize parameters, including initial position vector x^0, sensing range r^0 and initial searching step size s^0, number of beetles n, probability ε, total iteration number T, and establish a fitness function $f(x^t)$ for maximum or minimum searching results evaluating, where $x^t = [x^1, x^2, \ldots, x^n]^{\mathrm{T}}$.

Step 2. Search optimal in variable space according to

$$\begin{aligned} \boldsymbol{x}_r &= \boldsymbol{x}^t + r^t \mathbf{b} \\ \boldsymbol{x}_l &= \boldsymbol{x}^t - r^t \mathbf{b} \end{aligned} \tag{7}$$

where, t is the current iteration number; x_r and x_l are two positions (or solutions) lying in the right-hand and left-hand searching space respectively; $\mathbf{b}$ is a randomly generated direction vector for each beetle to do the current search.

Definitely, according to Equation (8), the sensing range r of antennae corresponding to the exploit ability, which should be large enough at the beginning to cover an appropriate searching area to be able to jump out of local minimum and then attenuate as time elapses to ensure that fine-grained searches can be performed near the optimal value.

$$r^t = 0.95 r^{t-1} + r^0 \tag{8}$$

where, r^0 guarantees the searching area shall not reduce to zero.

Step 3. Update the positions according to

$$\boldsymbol{x}^t = \boldsymbol{x}^{t-1} + s^t \mathbf{b}\ \mathrm{sign}\left(f(\boldsymbol{x}_r) - f(\boldsymbol{x}_l)\right) \tag{9}$$

where, the searching step size $s^t = 0.95 s^{t-1}$ is decreased while the search progresses, which is larger at the beginning of the search and the later the smaller; sign(.) is a sign function returns 1, 0, and -1 based on the difference between $f(\boldsymbol{x}_r)$ and $f(\boldsymbol{x}_l)$.

$$\mathrm{sign}(f(\boldsymbol{x}_r) - f(\boldsymbol{x}_l)) = \begin{cases} +1, & f(\boldsymbol{x}_r) - f(\boldsymbol{x}_l) > 0 \\ 0, & f(\boldsymbol{x}_r) - f(\boldsymbol{x}_l) = 0 \\ -1, & f(\boldsymbol{x}_r) - f(\boldsymbol{x}_l) < 0 \end{cases} \tag{10}$$

Step 4. Calculate the fitness function values and record the best position for the next step of searching.

Repeat Step 2 to Step 4 until the optimal (maximum or minimum) is found or the stop criterion is matched, and finally output the results.

2) MODIFICATION OF THE SEARCHING STEP SIZE

Clearly, by analyzing the original BAS and BSAS algorithms, a larger searching size helps the algorithm to jump out of local optimum status, but it would reduce the precision and speed of the convergence. On the other hand, it is easy to get a local optimal with a smaller searching step size. Therefore, the key point is how to get an appropriate searching step size

to balance the quality of the solution and the convergence precision and speed.

According to the current searching progress, that is, the relationship between the number of iterations and the maximum number of iterations, the attenuation of search step s^t is performed according to Equation (11).

$$s^t = \frac{m}{x_{\text{best}}} \times \exp\left(-\xi \times \left(\frac{t}{T}\right)^{\alpha}\right) + s_{\min} \tag{11}$$

where, m belongs to (0,1) is a regulatory factor; x_{best} is the recorded optimal position so far, which is updated or kept after each search step by calculating the fitness of each beetle (see Step 4 in Section 2.2.1); ξ belongs to [0, 1] is the limiting factor; t and T are the current and the maximum iteration number; $s_{\min}$ is the minimum search step; α is an integer from 1 to 30, here, α is equal to 25.

C. BSAS-BASED PF ALGORITHM

As mentioned before, particle degeneracy and particle impoverishment are the drawbacks of the traditional PF, which would affect the state estimation accuracy in the filtering process. In this paper, a modified BSAS algorithm is introduced into PF to overcome the particle impoverishment caused by the resampling process. The main idea is to use the global optimal information to guide the movement of overall particles. We define the global optimal information β as follows:

$$\beta_i = e^{-d_i^2} \tag{12}$$

where, d_i represents the Euclidian distance between the position of the ith beetle and the best position. Clearly, the larger d_i is, the smaller β_i is. As seen from PF algorithm theory, particles in the high probability density (HPD) region would help to perform high accuracy estimation. Therefore, if new particles are not obtained by resampling, how to place or move most of the existing particles into the HPD region is the key direction of performance improvement research. In that way, the global optimal information β could be used as a guide for particle movement. A particle with a larger β_i means it is located in or close to the HPD region, and its displacement distance should be shorter, vice versa.

Hence, the beetles (now they are particles) take the move action according to Equation (13), which guarantees the particles in the low probability density (LPD) region are adjusted to the high probability density (HPD) region, and thus, the particle diversity and impoverishment are also improved.

$$x_k^i = x_k^i + \beta_i(x_{\text{best}} - x_k^i) + \delta(rand - \frac{1}{2}) \tag{13}$$

where, $\delta = 0.4$ is a disturbance factor, and $rand$ is a random number that belongs to [0, 1].

Theoretically, firstly, because there is only one global optimal value of BSAS optimization, particle i in particle filter only needs to compare with the global optimal value, which avoids the high-order interactive operation and repeated calculation of attraction between particles. The computational complexity in this stage can be reduced from the original $O(N^2)$ to $O(N)$, thus ensuring the real-time performance of the filtering algorithm. Secondly, by using the global optimal value to do information exchange with particle i is essentially to use the global optimal value to guide the overall movement of the beetle swarm (or particles), which can significantly improve the global optimization ability of the BSAS optimization part, and thus can significantly reduce the probability of local extremum. Finally, the improved idea can make the filtering algorithm find a better value with fewer iterations and particle numbers. On the other hand, it reduces the computational complexity of particle filter and makes it easier to implement in engineering application.

The main steps of the improved BSAS-based PF are shown as bellows:

Step 1. Extract n particles (beetles) according to the predicting Equation (3) from the transition probability density;

Step 2. Use the modified BSAS algorithm to find the best position (the particle with the best fitness according to Equation (14));

$$\min_i E(z_{k,\text{new}} - z^i_{k,\text{predicted}})^2 \tag{14}$$

where, $z_{k,\text{new}}$ is the latest observation value and $z_{k,\text{predicted}}$ is the predicted observation value of the filter respectively.

Step 3. Calculate the global optimal information according to Equation (12);

Step 4. Move the particles toward the best position according to Equation (13);

Step 5. Update the sample weights and normalizing them according to Equation (4) and Equation (5);

Step 6. State estimating according to Equation (6), based on the least mean square error.

D. DFIG MODELLING

A state space model is needed to filtering state estimation work here. The simplified ideal state space model of DFIG used in this paper is derived from the physical model [30], [31] of DFIG based on the voltage equations of the stator and rotor. Assumed that: i) the stator and rotor windings are symmetrical and symmetrically fed; ii) Saturation of the inductances, iron losses, skin effect, and bearing friction is neglected; and iii) The winding resistance is considered to be constant. See more information in Rothenhagen and Fuchs [30].

In this paper, we consider that i) the DFIG operates at a fixed-speed and ii) the rotor voltages from the rotor-side convertor as control signals to regulate the wind turbine generator, while the stator voltages from the three-phase grid are as external known-inputs. Currents in the winding both in stator and rotor, which are supposed to be measured, determine the generated power. The model of DFIG is transformed in d-q reference frame, in which, the d-axis is chosen to coincide with stator phase r-axis at $t = 0$ and the q-axis leads the d-axis by 90 degrees in the direction of rotation. Equation (15) shows the generalized description. Where, the vector $x(t) = [I_{\text{Sd}} I_{\text{Sq}} I_{\text{Rd}}\ I_{\text{Rq}}]^{\text{T}}$ is the stator and rotor currents are

defined as states, and $u(t) = [U_{\mathrm{Rd}} U_{\mathrm{Rq}}]^{\mathrm{T}}$ is the rotor voltages are defined as control inputs.

$$\begin{cases} \dot{x}(t) = Ax(t) + Bu(t) + Ds(t) \\ y(t) = Cx(t) + Ff(t) \end{cases} \tag{15}$$

In which, $s(t) = [U_{\mathrm{Sd}} U_{\mathrm{Sq}}]^{\mathrm{T}}$ is the stator voltages are defined as external known-inputs; $y(t) = [y_0\ y_1\ y_2\ y_3]^{\mathrm{T}}$ is the output vector; $f(t) = [f_0\, f_1\, f_2\, f_3]^{\mathrm{T}}$ is the fault vector; and

$$A = \begin{bmatrix} -\frac{R_S}{\sigma L_S} & \frac{\omega_R L_m^2 n_p}{\sigma L_S L_R} & \frac{L_m R_R}{\sigma L_S L_R} & \frac{\omega_R L_m n_p}{\sigma L_S} \\ -\frac{\omega_R L_m^2 n_p}{\sigma L_S L_R} & -\frac{R_S}{\sigma L_S} & -\frac{\omega_R L_m n_p}{\sigma L_S} & \frac{L_m R_R}{\sigma L_S L_R} \\ \frac{L_m R_S}{\sigma L_S L_R} & -\frac{\omega_R L_m n_p}{\sigma L_R} & -\frac{R_R}{\sigma L_R} & -\frac{\omega_R n_p}{\sigma} \\ \frac{\omega_R L_m n_p}{\sigma L_R} & \frac{L_m R_S}{\sigma L_S L_R} & \frac{\omega_R n_p}{\sigma} & -\frac{R_R}{\sigma L_R} \end{bmatrix} \tag{16}$$

where in Equations (16) to (18), $R_S = 0.0071\ \Omega$ and $R_R = 0.005\ \Omega$ represent the stator and rotor per phase resistance respectively; $L_S = 0.171$ H and $L_R = 0.159$ H represent the cyclic stator and rotor inductances respectively; Constant ω_R is the mechanical rotor frequency (speed); $n_p = 2$ is the number of pole pairs. The mutual inductance is written as L_m equals to 2.9 H and σ is defined by Equations (20).

$$B = \begin{bmatrix} -\frac{L_m}{\sigma L_S L_R} & 0 \\ 0 & -\frac{L_m}{\sigma L_S L_R} \\ \frac{1}{\sigma L_R} & 0 \\ 0 & \frac{1}{\sigma L_R} \end{bmatrix} \tag{17}$$

$$D = \begin{bmatrix} \frac{1}{\sigma L_S} & 0 \\ 0 & \frac{1}{\sigma L_S} \\ -\frac{L_m}{\sigma L_S L_R} & 0 \\ 0 & -\frac{L_m}{\sigma L_S L_R} \end{bmatrix} \tag{18}$$

$$C = F = \begin{bmatrix} 1 & 0 & 0 & 0 \\ 0 & 1 & 0 & 0 \\ 0 & 0 & 1 & 0 \\ 0 & 0 & 0 & 1 \end{bmatrix} \tag{19}$$

$$\sigma = 1 - L_m^2 L_S^{-1} L_R^{-1} \tag{20}$$

Equation (19) means that all currents are measurable as assumed and the faults are settable. Definitions of the four elements (f_0 to f_3) in the fault vector F are as follows: f_0 represents normal (fault-free status); f_1 to f_3 represent man-made fault status. Respectively, f_1 stands for a short circuit fault shown in Equation (21), f_2 stands for a bias fault shown in Equation (22), and f_3 stands for a gain fault shown in Equation (23), where μ is a degree factor.

$$R_{Rf} = (1 - \mu) R_R, \quad 0 < \mu < 1 \tag{21}$$

$$I_{Rf} = I_R + 2 \tag{22}$$

$$I_{Rf} = 2 I_R \tag{23}$$

Since the PF algorithm operates in discrete time, the continuous dynamical system presented previously in Equation (15) needs to be discretized, which is shown as follows:

$$\begin{cases} x_{k+1} = A_{\mathrm{d}} x_k + B_{\mathrm{d}} u_k + D_{\mathrm{d}} s_k \\ y_k = C_{\mathrm{d}} x_k + F_{\mathrm{d}} f_k \end{cases} \tag{24}$$

where, the coefficients of the matrices depend on the sampling time, therefore, they are not given in this paper. The discrete mathematical model of DFIG, shown in Equation (24), enables its integration with the filtering algorithms discussed in Section 2.3.

III. RESULTS AND DISCUSSIONS

A. PERFORMANCE VERIFY OF THE MODIFIED BSAS OPTIMIZATION ALGORITHM

In this section, we will test the optimization performance of the modified BSAS algorithm to verify the convergence and optimization effect of the algorithm. Stronger optimization ability promises the algorithm can search for the optimal particles when applied to improve particle filter. Testing the newly modified BSAS optimization algorithm based on three selected standard functions shown in Equations (25), (26), and (27).

$$f_{\mathrm{Schaffer}}(x_1, x_2) = 0.5 - \frac{\sin^2(x_1^2 - x_2^2) - 0.5}{[1 + 0.001(x_1^2 + x_2^2)]^2} \tag{25}$$

$$f_{\mathrm{Michalewicz}}(x_1, x_2) = -\sum_{i=1}^{2} \sin(x_i)(\sin(ix_i^2/\pi))^{20} \tag{26}$$

$$f_{\mathrm{Step}}(x_1, x_2) = \sum_{i=1}^{2} (|x_i + 0.5|)^2 \tag{27}$$

Schaffer function (Equation (25)) f_{Schaffer} has a global maximum value of 1 at $(x_1, x_2) = (0, 0)$ on the squared search domain x_i belongs to $[-10, 10]$ for both $i = 1$, and $i = 2$.

Michalewicz function (Equation (26)) $f_{\mathrm{Michalewicz}}$ has a global minimum value of -1.8013 at $(x_1, x_2) = (2.20, 1.57)$ on the hypercube x_i belongs to $[0, 5]$ for both $i = 1$, and $i = 2$.

Step function (Equation (27)) f_{Step} has a global minimum value of 0 at $(x_1, x_2) = (-0.5, -0.5)$ on the squared search domain x_i belongs to $[-5, 5]$ for both $i = 1$, and $i = 2$.

All the three functions pose a risk for optimization algorithms, particularly hillclimbing algorithms, to be trapped in one of its many local minima. All the results are shown in Figures 3 to 8.

Result figures illustrate that the newly improved optimization algorithm has good performance in finding the optimal results based on the challenge test functions verifying. As seen from the figures, it always can get the maximum or minimum value of the three test functions. This also provides a reliable basis for the algorithm in the process of subsequent optimization of the particle filter.

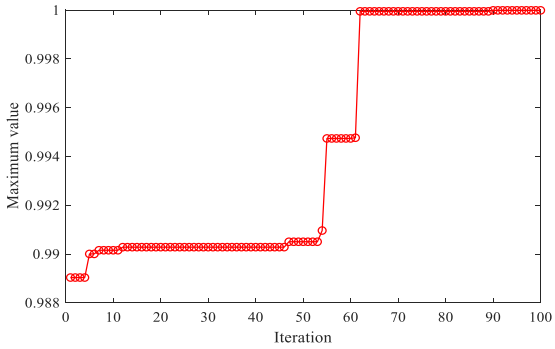

FIGURE 3. Optimizing iterative process of the Schaffer function.

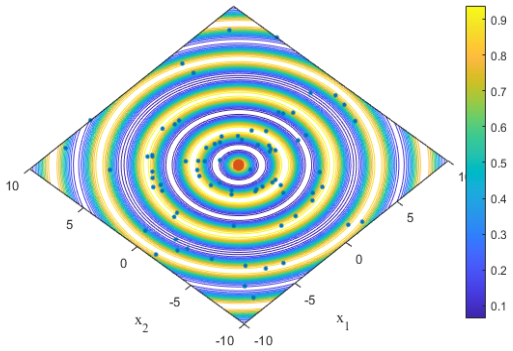

FIGURE 4. Optimization results of the Schaffer function. (The optimal solution is shown in the large orange dot at (0, 0)).

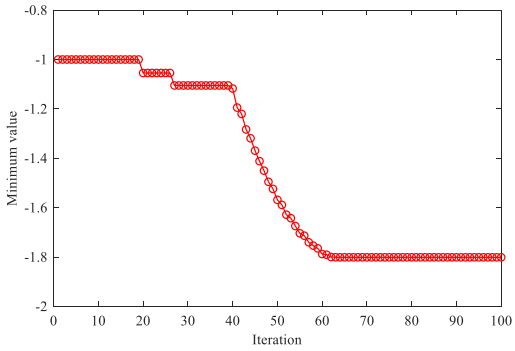

FIGURE 5. Optimizing iterative process of the Michalewicz function.

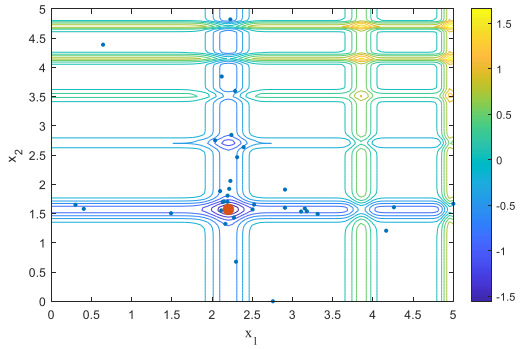

FIGURE 6. Optimization results of the Michalewicz function. (The optimal solution is shown in the large orange dot at (2.2016, 1.5708)).

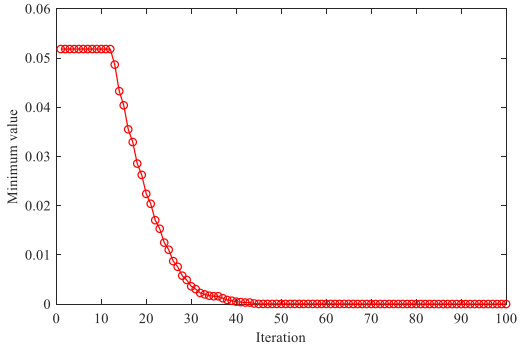

FIGURE 7. Optimizing iterative process of the Step function.

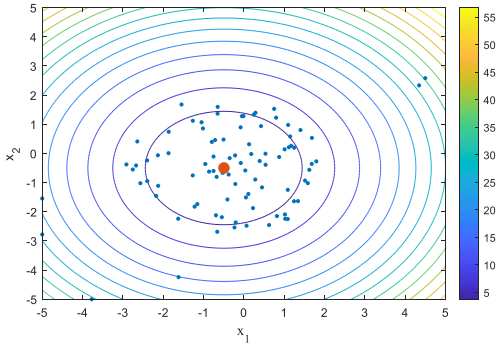

FIGURE 8. Optimization results of the Step function. (The optimal solution is shown in the large orange dot at (−0.4994, −0.5011)).

B. STATE ESTIMATION EXPERIMENT OF THE MODIFIED BSAS BASED PF ALGORITHM

Based on the above performance results of the modified BSAS optimization algorithm in optimal searching tests, further tests on state estimation of the improved particle filter algorithm (BSAS-based PF) are conducted in this section. The followed system model (28) is widely used in the evaluation of PF-based estimation methods in econometrics. It has the characteristics of high nonlinearity and double peaks. It is difficult for traditional filtering methods to achieve effective state tracking.

$$\begin{cases} x_{k+1} = \frac{x_k}{2} + \frac{25x_k}{1+x_k^2} + 8\cos 1.2k + n_k \\ y_k = \frac{x_k^2}{20} + v_k \end{cases} \tag{28}$$

where, n_k and v_k are independent noises.

Seen from the compared results shown in Figure 9, BAPF and GRPF perform well at the estimating work, they all can track the state dynamics in the simulation process, because they can also inhibit particle degradation based on their own improvement principles. However, in the simulation study, the BSAS-based PF algorithm always has the best performance in most cases and it can track the state more accurately

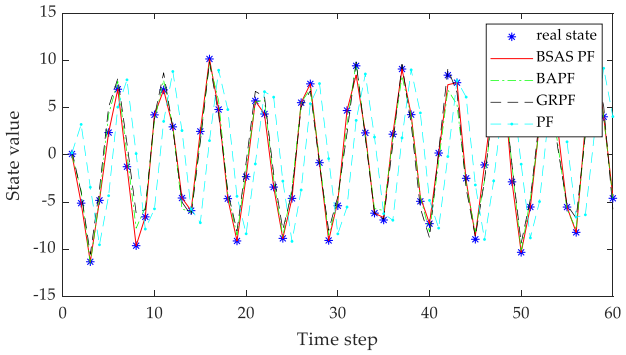

FIGURE 9. Compared results of state estimation when the number of particles is 100. (BAPF: particle filter based on bat algorithm [32]; GRPF: genetic resampling particle filter [33]; PF: particle filter [14]; BSAS PF: BSAS-based PF algorithm proposed in this work).

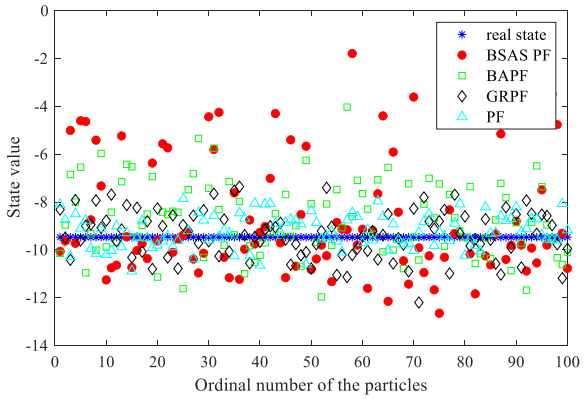

FIGURE 10. Compared results of the distribution of all the 100 particles at time $k = 45$.

TABLE 1. RMSE error of the four algorithms.

(N, Q)	PF	GRPF	BAPF	Proposed
(20, 1)	6.8433	1.4545	1.9437	0.7105
(50, 1)	6.7366	1.3948	1.1290	0.2416
(100, 1)	6.6075	1.2107	0.8197	0.1547
(20, 5)	7.5546	2.4264	4.0005	1.5955
(50, 5)	7.4134	2.3589	2.9383	1.2312
(100, 5)	6.5767	1.9719	1.5140	1.1136

than them. That is, after the optimization of the particles' positions, more particles have been moved to the high likelihood region, which is helpful for getting better results in the state estimation work, and avoiding the particle degeneracy with the iterations going on.

Figure 10 shows the compared results of the distribution of all the 100 particles at time $k = 45$. BSAS-based PF can keep most of the particles around the real state of the system. Besides, there are still some of the particles that are away from the real state at the current time, this distribution appearance can assure the estimation accuracy of the filter at the next time step once the system has a jump. Actually, BSAS-based PF performance a good estimation result, shown in Figure 9, even the system state jumped a lot at each time step, while the other compared algorithms have not so widely distributed particles.

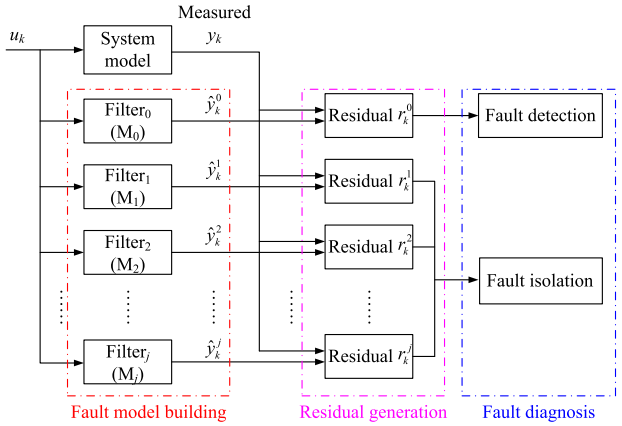

FIGURE 11. Fault diagnosis implementation based on particle filter.

To verify the estimation accuracy of the four algorithms, more simulation results were obtained based on different particle numbers (N) and different noise variance (Q) as shown in Table 1. The estimation accuracy of the algorithm is evaluated by the root mean squared error (RMSE) which is defined as shown in Equation (29):

$$RMSE = \sqrt{\frac{1}{T}\sum_{t=1}^{T}(x_t - \hat{x}_t)^2} \tag{29}$$

where, T, equals to 60, is the iterative step number.

As shown in Table 1, the more the number of particles is, the better accuracy all the methods can achieve. Especially, it is interesting that GRPF performs better than BAPF when the number of particles is small, but as the number of particles increases, BAPF will perform better than GRPF conversely. On the whole, the modified BSAS-based PF shows the best performance regardless of the change of particle size or the noise variance among all the four methods in our testing experiments. It also shows that the improvement of PF algorithm in this paper is effective and significant.

C. FAULT DIAGNOSIS OF DFIG SYSTEM

Based on the model presented in Section 2, we incorporated the modified BSAS-based PF for the fault diagnosing work in DFIG-based wind turbine system.

The main implementation process of the fault diagnosis method based on particle filter includes the following three parts: fault model building, residual generation, and fault diagnosis (fault detection and isolation), which are shown in Figure 11. The fault diagnosis model set is established under the frame of the particle filter, including a normal state model (M_0) and several fault state models (M_1 to M_j). All fault state models are designed reasonably according to the equipment operation and fault mechanism and they are configured with an independent particle filter respectively to match the normal model and the fault model. Accordingly, each filter will match a set of specific fault modes to track the possible fault behavior mode of the system.

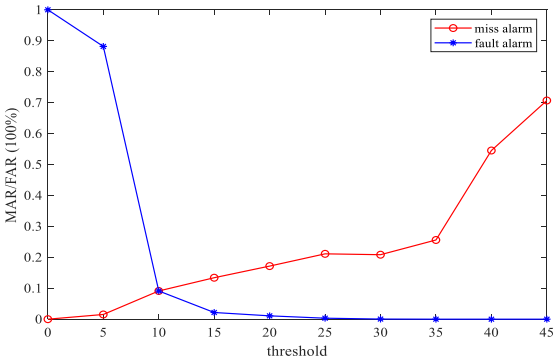

FIGURE 12. MAR and FAR with different thresholds.

Residuals mentioned in Figure 2 can be used as an indicator to detect faults, because the generated residuals are close to zero when the behavior of the monitored system is normal. On the contrary, when a fault occurs, the residuals will rise significantly away from zero, which indicates that the system state is distinguishable from the normal one. In the fault diagnosis implementation process shown in Figure 11, residuals are generated based on Equation (30).

$$r_k^i = y_k - \hat{y}_k^i \tag{30}$$

where, r_k^i is the residual of the ith model at time k, which is the difference between the observed output and the predicted output. Its value reflects the inconsistency between the actual operation status of the target system and the theoretical operation status of the mathematical model simulation. In general, we need to set a reasonable threshold and compare with it to determine whether or not the fault occurs and what fault occurs. Therefore, the fault can be observed and isolated by analyzing the residual.

1) FAULT THRESHOLD SELECTION

Firstly, the experiment of fault threshold selection is carried out to determine the threshold of residuals used in fault detection and isolation.

In this paper, the selection of fault threshold is determined by two important indexes, which are missing alarm rate (MAR) and false alarm rate (FAR) shown in Equations (31) and (32). MAR refers to the system is in fault but not detected; FAR refers to the system is normal but detected as failure. A fault diagnosis method should minimize both the MAR and the FAR as much as possible based on the consideration of performance balance.

$$MAR = \frac{N_{\mathrm{FN}}}{N_{\mathrm{F}}} \times 100\% \tag{31}$$

$$FAR = \frac{N_{\mathrm{NF}}}{N_{\mathrm{N}}} \times 100\% \tag{32}$$

where, N_{FN} is the number of faults identified as normal, N_{NF} is the number of normal identified as fault, N_{F} is the number of faults, N_{N} is the number of normal.

Figure 12 shows the results of MAR and FAR of fault f_3 under different thresholds. It can be seen that they show different trends with different thresholds. If the threshold setting becomes large, the FAR will increase while the MAR will decrease; vice versa. The experimental results show that when the threshold value is 10, the MAR and the FAR are the best balance points, both of them are 9.12%. Therefore, the fault threshold value shall be set to 10 for the better comprehensive performance of the method.

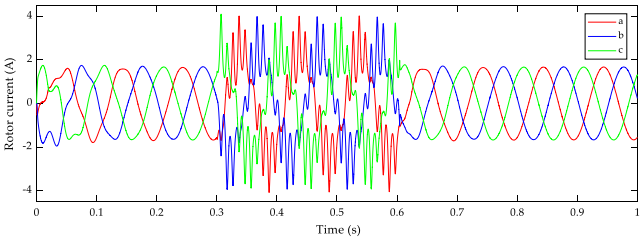

FIGURE 13. Rotor current short-circuit fault (f_1), where, $\mu = 0.5$.

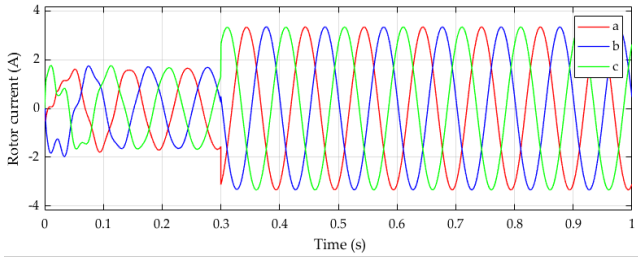

FIGURE 14. Rotor current gain fault (f_3).

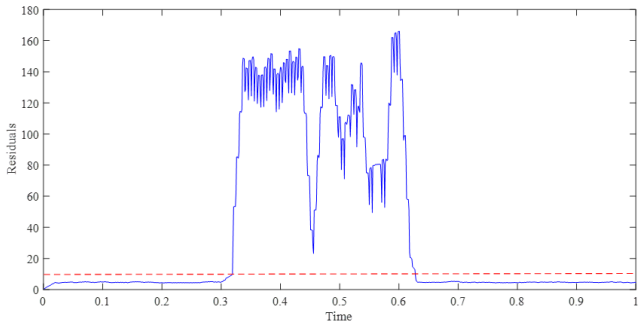

FIGURE 15. Fault detection results of f_1.

2) FAULT DETECTION

Take the short-circuit fault (f_1) and sensor constant gain fault (f_3) as examples to test the fault detection performance of the improved BSAS-based PF.

Figure 13 shows the appearance of the man-made rotor current fault (f_1) that occurs between the time periods 0.3s to 0.6s in three phase $a-b-c$ coordinate. Figure 14 shows the appearance of the man-made rotor current fault (f_3) starts from the time point 0.3s in three phase $a-b-c$ coordinate.

The fault detection result of the short-circuit fault f_1 based on the new improved algorithm is shown in Figure 15. The red dotted line is a fault threshold value.

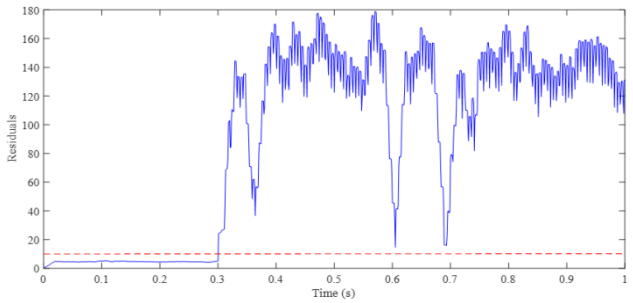

FIGURE 16. Fault detection results of f_3.

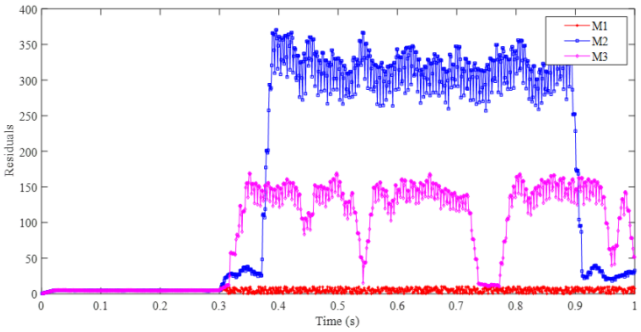

FIGURE 17. Residuals of the fault isolation simulation.

It can be seen from the figure that after a slight delay at 0.3 seconds, the residual rises sharply beyond the fault threshold, indicating that the system has a fault from this time on. This is consistent with the fault time we set. The result shows that the BSAS-PF algorithm can be used to detect a sudden change of the system state, quickly and accurately. Then, the residual value has been fluctuating over the threshold value for a while, which means that the system is staying in fault or the fault is not eliminated. When the fault is eliminated at 0.6 seconds, the system state changes suddenly again, and the residual value also changes immediately. Finally, the residual value tends to the normal range with the fault elimination. In case of two abrupt changes in the system, the BSAS-PF algorithm can track the faults timely and accurately, which verifies the effectiveness of the algorithm applied to the fault detection of the system.

The fault detection result of the gain fault f_3 based on the new improved algorithm is shown in Figure 16.

It can be seen from the figure that, at 0.3 seconds, with the occurrence of the manual setting gain fault, the system state changes abruptly, and the residual changes immediately too, which exceeds the fault threshold a lot. The system fault is detected. Different from the short-circuit fault f_1, after the gain fault f_3 occurs, the residual always fluctuates in the range beyond the threshold value, and does not recover to the fault threshold line, indicating that the current sensor is continuously in constant gain fault, which is completely consistent with the fault setting we made.

3) FAULT ISOLATION

After the fault is detected, all the particle filters are started to isolate the fault. Figure 17 is the result of all fault modes by running the particle filters. It can be seen that residuals of fault modes M_2 (bias fault f_2) and M_3 (gain fault f_3) are relatively large, while residuals of M_1 (short-circuit fault f_1) is the smallest. Hence, fault mode M_1 is determined that the system is in short-circuit fault f_1. The isolation process of other fault modes is similar to M_1.

Moreover, from all the results, high accuracy of state estimation ability can ensure the diagnosis efficiency. That is to say, if the estimation accuracy is poor, the residuals generated by the diagnosis system will be largely changed dynamically, which could lead to a false alarm of the fault when the DFIG system running in normal. Based on a proper threshold, the false-alarm rate can be reduced. However, it is difficult to setup a threshold properly, because there are many reasons (e.g. system noise, measurement error) that shall affect the values of residuals in fault diagnosis practicing. Therefore, an adaptive threshold shall be introduced into practicing of fault diagnosis system in the future study.

IV. CONCLUSION

Wind power systems are usually installed in remote areas with few people tread, it is necessary to develop a remote monitoring system and a reliable fault diagnosis algorithm to monitor important components and equipment in wind turbine systems. For DFIG fault diagnosis application in wind turbine systems, we have developed a modified BSAS-based particle filter algorithm.

i) We improved the optimal search performance of the beetle swarm antennae search (BSAS) algorithm based on an adaptively search step size. It shows good results in the optimization of three typical test functions.

ii) We introduced the improved BSAS algorithm to the traditional particle filter (PF) to overcome the drawbacks of particle diversity and impoverishment caused by the resampling process. Particles are moved to close to the high likelihood region by attraction, which can ensure the diversity of particles, reduce the degradation degree of particles and effectively improve the estimation accuracy. BSAS-based PF is verified by a state tracking simulation study. Results show that it has a better state estimating accuracy compared with PF, BAPF and GRPF methods.

iii) Based on the good state estimation ability, the BSAS-based PF is used to perform the fault diagnosis in a DFIG system. It can detect faults rapidly and accurately based on residual values, as well as in fault isolation. The proposed fault diagnostic method has an important theoretical significance and engineering application value.

REFERENCES

[1] S. T. Kandukuri, A. Klausen, H. R. Karimi, and K. G. Robbersmyr, "A review of diagnostics and prognostics of low-speed machinery towards wind turbine farm-level health management," *Renew. Sustain. Energy Rev.*, vol. 53, pp. 697–708, Jan. 2016.

[2] *Global Wind Report 2018*, Global Wind Energy Council (GWEC), Brussels, Belgium, Apr. 2019.

[3] *Global Renewables Outlook: Energy Transformation 2050*, International Renewable Energy Agency (IRENA), Abu Dhabi, United Arab Emirates, Apr. 2020.

[4] J. Nilsson and L. M. Bertling, "Survey of failures in wind power systems with focus on Swedish wind power plants during 1997–2005," *IEEE Trans. Energy Convers.*, vol. 22, no. 1, pp. 167–173, Mar. 2007.
[5] J. Zeng, Y. Chen, P. Yang, and H. Guo, "Review of fault diagnosis methods of large-scale wind turbines," *Power Syst. Technol.*, vol. 42, no. 3, pp. 849–860, Mar. 2018.
[6] J. P. Salameh, S. Cauet, E. Etien, A. Sakout, and L. Rambault, "Gearbox condition monitoring in wind turbines: A review," *Mech. Syst. Signal Process.*, vol. 111, pp. 251–264, Oct. 2018.
[7] W. Y. Liu, B. P. Tang, J. G. Han, X. N. Lu, N. N. Hu, and Z. Z. He, "The structure healthy condition monitoring and fault diagnosis methods in wind turbines: A review," *Renew. Sustain. Energy Rev.*, vol. 44, pp. 466–472, Apr. 2015.
[8] W. Mao, W. Feng, and X. Liang, "A novel deep output kernel learning method for bearing fault structural diagnosis," *Mech. Syst. Signal Process.*, vol. 117, pp. 293–318, Feb. 2019.
[9] B. Boulkroune, M. Galvez-Carrillo, and M. Kinnaert, "Combined signal and model-based sensor fault diagnosis for a doubly fed induction generator," *IEEE Trans. Control Syst. Technol.*, vol. 21, no. 5, pp. 1771–1783, Sep. 2013.
[10] X. S. Ding, *Model-Based Fault Diagnosis Techniques: Design Schemes, Algorithm, and Tools*. Berlin, Germany: Springer, 2008.
[11] Q. Zhang, "A new residual generation and evaluation method for detection and isolation of faults in non-linear systems," *Int. J. Adapt. Control Signal Process.*, vol. 14, no. 7, pp. 759–773, Jul. 2015.
[12] A. Doucet, S. J. Godsill, and C. Andrieu, "On sequential Monte Carlo sampling methods for Bayesian filtering," *Statist. Comput.*, vol. 10, pp. 197–208, Jul. 2000.
[13] M. S. Arulampalam, S. Maskell, N. Gordon, and T. Clapp, "A tutorial on particle filters for online nonlinear/non-Gaussian Bayesian tracking," *IEEE Trans. Signal Process.*, vol. 50, no. 2, pp. 174–188, Feb. 2002.
[14] M. Speekenbrink, "A tutorial on particle filters," *J. Math. Psychol.*, vol. 73, pp. 140–152, Aug. 2016.
[15] H. Bi, J. Ma, and F. Wang, "An improved particle filter algorithm based on ensemble Kalman filter and Markov chain Monte Carlo method," *IEEE J. Sel. Topics Appl. Earth Observ. Remote Sens.*, vol. 8, no. 2, pp. 447–459, Feb. 2015.
[16] N. Gordon, D. Salmond, and A. F. M. Smith, "Novel approaches to nonlinear/non-Gaussian Bayesian state estimation," *Radar Signal Process. IEE Proc. F*, vol. 140, no. 2, pp. 107–113, May 1993.
[17] S. Yin and X. Zhu, "Intelligent particle filter and its application to fault detection of nonlinear system," *IEEE Trans. Ind. Electron.*, vol. 62, no. 6, pp. 3852–3861, Jun. 2015.
[18] B. Liu, C. Shi, and Y. Shi, "Particle filter optimization: A brief introduction," in *Proc. Int. Conf. Swarm Intell.*, Brussels, Belgium, 2016, pp. 1–10.
[19] F. Wang, M. Lu, Q. Zhao, and Z. Yuan, "Particle filtering algorithm," *Chin. J. Comput.*, vol. 37, no. 8, pp. 1679–1694, Aug. 2014.
[20] C. Huemmer, C. Hofmann, R. Maas, and W. Kellermann, "Estimating parameters of nonlinear systems using the elitist particle filter based on evolutionary strategies," *IEEE/ACM Trans. Audio, Speech, Lang. Process.*, vol. 26, no. 3, pp. 595–608, Mar. 2018.
[21] S. Cheng and J. Zhang, "Review on particle filters," *J. Astronaut.*, vol. 29, no. 4, pp. 1109–1111, Jul. 2008.
[22] X. Yang, Q. Pan, R. Wang, and H. Zhang, "Development and prospect of particle filtering," *Control Theory Appl.*, vol. 23, no. 2, pp. 261–267, Apr. 2006.
[23] X. Wang, T. Li, S. Sun, and J. Corchado, "A survey of recent advances in particle filters and remaining challenges for multitarget tracking," *Sensors*, vol. 17, no. 12, p. 2707, Nov. 2017.
[24] R. Zhou, B. Liu, and J. Teng, "Improved resampling particle filter for maneuvering point target tracking," *J. Appl. Sci.*, vol. 13, no. 11, pp. 2045–2050, May 2013.
[25] M. Ahwiadi and W. Wang, "An enhanced mutated particle filter technique for system state estimation and battery life prediction," *IEEE Trans. Instrum. Meas.*, vol. 68, no. 3, pp. 923–935, Mar. 2019.
[26] N. Daroogheh, N. Meskin, and K. Khorasani, "A dual particle filter-based fault diagnosis scheme for nonlinear systems," *IEEE Trans. Control Syst. Technol.*, vol. 26, no. 4, pp. 1317–1334, Jul. 2018.
[27] K. Li, J. Wu, Q. Zhang, L. Su, and P. Chen, "New particle filter based on GA for equipment remaining useful life prediction," *Sensors*, vol. 17, no. 4, p. 696, Mar. 2017.
[28] J. Wang and H. Chen, "BSAS: Beetle swarm antennae search algorithm for optimization problems," Jul. 2018, pp. 1–4, *arXiv:1807.10470*. [Online]. Available: https://arxiv.org/abs/1807.10470
[29] X. Jiang and S. Li, "BAS: Beetle antennae search algorithm for optimization problems," *Int. J. Robot. Control*, vol. 1, no. 1, pp. 1–5, Apr. 2018.
[30] K. Rothenhagen and F. W. Fuchs, "Current sensor fault detection by bilinear observer for a doubly fed induction generator," in *Proc. 32nd Annu. Conf. IEEE Ind. Electron. (IECON)*, Paris, France, Nov. 2006, pp. 1–6.
[31] K. Rothenhagen and F. W. Fuchs, "Current sensor fault detection, isolation, and reconfiguration for doubly fed induction generators," *IEEE Trans. Ind. Electron.*, vol. 56, no. 10, pp. 4239–4245, Oct. 2009.
[32] Z. M. Chen, M. C. Tian, P. L. Wu, Y. M. Bo, F. F. Gu, and C. Yue, "Intelligent particle filter based on bat algorithm," *Acta Phys. Sinica*, vol. 66, no. 5, pp. 41–50, May 2017.
[33] L. Ye, J. Wang, and Q. Zhang, "Genetic resampling particle filter," *Acta Automatica Sinica*, vol. 33, no. 8, pp. 885–887, Aug. 2007.

ZHENG CAO was born in Dingxi, Gansu, China, in 1979. He received the B.S. and M.S. degrees in control engineering from the Lanzhou University of Technology, China, in 2002 and 2011, respectively, where he is currently pursuing Ph.D. degree in control engineering.

Since 2012, he has been a Lecturer with the College of Electrical and Information Engineering, Lanzhou University of Technology. He is the author of two books, more than 15 articles, two inventions, and seven patents. His research interests include wind power system modeling and control, fault diagnosis and prognosis, artificial intelligence, and pattern recognition.

Mr. Cao has received several prizes, including a Second Prize of the Science and Technology Progress Awards of Gansu Province in 2013, a First Prize of the "Internet +" Innovation and Entrepreneurship Competition in 2019, and a Third Prize of the Science and Technology Progress Award of Colleges and Universities in Gansu Province in 2018.

XIANJUN DU was born in Hangzhou, Zhejiang, China, in 1979. He received the B.S. and M.S. degrees in electrical engineering and the Ph.D. degree in control engineering from the Lanzhou University of Technology, China, in 2002, 2008, and 2013, respectively.

Since 2014, he has been an Assistant Professor with the College of Electrical and Information Engineering, Lanzhou University of Technology. From 2016 to 2018, he was a Visiting Scholar with the Water: Effective Technologies and Tools (WETT) Research Centre, RMIT University, Melbourne, Australia. He is the author of three books, more than 40 articles, two inventions, and four patents. His research interests include fault diagnosis and prognosis, system modeling, optimization and control, artificial intelligence, neural computing, and deep learning.

Dr. Du received two second prize of the Science and Technology Progress Award of Gansu Province, in 2013 and 2015.